Desalination and Water Treatment
www.deswater.com

doi: 10.5004/dwt.2022.28503

261 (2022) 159–169
June

Efficient adsorption of nitrate and phosphate from wastewater by the cost-effective Mg/Ca bimetallic oxide composites functionalized peanut shell

Li Han[a], Renrong Liu[a], Huifang Wang[a], Baowei Hu[a], Muqing Qiu[a,*], Hao Zhang[b]

[a]*School of Life Science, Shaoxing University, Shaoxing 312000, China, email: qiumuqing@usx.edu.cn (M. Qiu)*
[b]*Key Laboratory of Agro-Ecological Processes in Subtropical Region, Institute of Subtropical Agriculture, Chinese Academy of Sciences, Changsha 410125, China*

Received 10 December 2021; Accepted 7 April 2022

ABSTRACT

Large amounts of nitrogen and phosphorus elements were discharged into the environment. They would lead to severe eutrophication of water bodies. The development of economically efficient, green and ecological adsorbents is the current focus for adsorption technology. In this research, the cost-effective biochar modified by Mg/Ca bimetallic oxide composites (Mg/Ca@PS) for adsorption of NO_3^- and PO_4^{3-} ions in aqueous solution was investigated. Additionally, Mg/Ca@PS also was characterized by scanning electron microscopy, transmission electron microscopy, energy-dispersive X-ray analysis, X-ray diffraction, and Fourier-transform infrared spectroscopy, respectively. The experimental results showed that the adsorption process of NO_3^- ions in aqueous solution by Mg/Ca@PS could be described by pseudo-second-order kinetic model and Langmuir isotherm model, respectively. However, the adsorption process of PO_4^{3-} ions in solution by Mg/Ca@PS could be described by pseudo-second-order kinetic model and Freundlich isotherm model, respectively. Additionally, the adsorption capacity of NO_3^- and PO_4^{3-} ions in aqueous solution by Mg/Ca@PS were 18.52 and 47.85 mg/g, respectively. The adsorption mechanisms of NO_3^- ions and PO_4^{3-} ions in solution by Mg/Ca@PS mainly contain surface adsorption, intraparticle diffusion, electrostatic attraction, and ion exchange. Moreover, the adsorption mechanism of PO_4^{3-} ions in solution by Mg/Ca@PS also includes chemical precipitation. In the five recycle times, the removal rate of NO_3^- and PO_4^{3-} ions still reached 55.31% and 48.12%, respectively. It indicated that the chemical stability of Mg/Ca@PS was very well, and it was a good environmental friendly material.

Keywords: Adsorption; Nitrate and phosphate; Mg/Ca bimetallic oxide composites; Peanut shell

1. Introduction

With the rapid development of industry and agriculture, large amounts of nitrogen (N) and phosphorus (P) elements are discharged into the environment [1]. They would lead to severe eutrophication of water bodies. The main forms of these N and P elements in water body were NO_3^-, NH_4^+, and PO_4^{3-}, respectively [2,3]. Therefore, efficient treatment of nitrogen and phosphorus elements in water body has become a research hotspot in the field of environment science. At present, many scholars have begun to study this problem. Therefore, the development of highly efficient and low-cost treatment technologies is urgently required for N and P removal from wastewater [4]. At present, the treatment technologies for nitrogen and phosphorus removal in water mainly include membrane separation method, struvite crystallization method, plant adsorption method and adsorption–desorption method [5]. Among of these treatment technologies, the adsorption method can not only remove the elements of nitrogen and phosphorus, but also the adsorbent materials can be used as a fertilizer for soil [6]. Therefore, adsorption method has been received the attention of many scholars. Adsorption material is very

* Corresponding author.

important for adsorption method. However, adsorption material, such as activated carbon, clay minerals, and zeolites, is usually expensive and with low adsorbent capacity and selectivity. Therefore, the development of suitable adsorption material is very important for the successful application of adsorption method in pollutants removal.

Biochar is an efficient and cheap adsorption material, which is a by-product of pyrolyzed biomass [7–9]. Biochar contains the characteristics of high specific surface area, low price, simple operation and high adsorption capacity. Therefore, it can be used as adsorbent material [10,11]. A large number of researches indicate that biochar could been widely used for removal of heavy metals, radionuclides, organic pollutants, inorganic pollutants, and so on [12–18]. Additionally, biochar also has been widely applied in the N and P removal in solution [19]. However, the adsorption capacity of the unmodified biochar for N and P in solution removal is usually very low. Therefore, it is necessary to modify biochar in order to improve its adsorption performance. For example, Wu et al. [20] synthesized the modified biochar from rice straw by iron (II/III). After biochar was modified with iron (II/III), the adsorption capacity of P in solution removal by the modified biochar increased from 16.4 to 39.2 mg/g. Zheng et al. [21] reported that Mg–Al-modified biochar from wheat straw was obtained through modified by Mg/Al composites. The adsorption capacity of Mg–Al-modified biochar for phosphate removal was elaborated in details. The experimental results showed the adsorption capacity of phosphate removal by the modified biochar increased significantly [20,22–24]. The elements of Ca and Mg are non-toxic and widely present in nature, and they are considered to be promising materials for the modification of biochar. Some researches on the adsorption of pollutants by biochar modified with the element of Ca or Mg have been reported. However, the adsorption of N and P in solution by biochar modified with Ca and Mg composites are fewer.

The cost-effective biochar modified by Mg/Ca bimetallic oxide composites (Mg/Ca@PS) was prepared. Then, the adsorption experiments of N and P in solution by Mg/Ca@PS are carried out. The main objectives are to be achieved: (1) Preparation of a cost-effective Mg/Ca@PS; (2) Characterization of Mg/Ca@PS; (3) Adsorption processes of NO_3^- and PO_4^{3-} ions in solution by Mg/Ca@PS; (4) Proposed mechanism between Mg/Ca@PS and NO_3^- or PO_4^{3-} ions in solution.

2. Materials and methods

2.1. Materials

Peanut shells are collected from a farm in Jinan City, Shandong Province. Chemical reagents, such as $CaCl_2$, $MgCl_2$, H_2SO_4, NaOH, $NaNO_3$ and KH_2PO_4, are purchased from Shanghai Macklin Biochemical Co. Ltd., and they are all analytical grade. The distilled water is used for the total experiments.

2.2. Preparation of Mg/Ca@PS

Peanut shell is used as the raw material of biochar. The peanut shells are washed for three times with clean water. Then they are dried in an oven at 110°C for 12 h. The dried peanut shells are grounded, and sieved into mesh #100. The biochar from peanut shell (PS) is prepared with the method of high-temperature pyrolysis. In a word, they are pyrolyzed in a muffle furnace for 2 h at 500°C under N_2 condition (100 mL/min). The cost-effective Mg/Ca bimetallic oxide composites functionalized peanut shell (Mg/Ca@PS) is prepared by an impregnation method. Briefly, the peanut shell powder is soaked in the 100 mL of mixture solution (1 mol/L $MgCl_2$ and 1 mol/L $CaCl_2$). Add 100 mL 4 mol/L NaOH, and place them in the shaker for 24 h at 200 rpm and 25°C. After the mixture is filtered, they are washed with distilled water for three times in order to remove the Ca^{2+} and Mg^{2+} ions on the particle surface. Then, they are dried in an oven at 110°C for 12 h, and they are pyrolyzed in a muffle furnace for 2 h at 500°C under N_2 condition (100 mL/min). The adsorbent of Mg/Ca@PS is obtained. They will be used for removal of nitrogen and phosphorus in solution. The synthesis pathway for Mg/Ca@PS is displayed in Fig. 1.

2.3. Characterization of sorbents

The characterization of PS and Mg/Ca@PS are determined by scanning electron microscopy (SEM), transmission electron microscopy (TEM), N_2-Brunauer–Emmett–Teller adsorption, Fourier-transform infrared spectroscopy (FT-IR), X-ray diffractometer (XRD) and X-ray photoelectron spectrometer (XPS) respectively. The detailed information is provided in Supporting Information.

2.4. Adsorption experiments

Adsorption experiments are all carried out in 250 mL Erlenmeyer flasks at 150 rpm under a constant temperature condition. The detailed information is provided in Supporting Information. In a word, the certain amount of the adsorbent is added into a 250 mL Erlenmeyer flask containing 100 mL initial concentration of NO_3^- or PO_4^{3-} ions. Flask is sealed by bottle cap and placed in the shaker at 150 rpm and constant temperature. The deionized water is used in all adsorption experiments. The pH in solution is adjusted with the 0.1 mol/L NaOH or 0.1 mol/L HCl solution. When the entire adsorption process reaches equilibrium, the supernatant is collected through filter filtration. The total nitrogen (TN) and total phosphorus (TP) concentration in the supernatant are analyzed by UV-Vis spectrophotometry, respectively [25]. The residual sample is centrifuged at 3,000 rpm for 5 min. Sediment is determined by microscopic technologies. All experiments are carried out in duplicate and the data are analyzed by the mean and standard deviation. Additionally, calculations of the removal efficiency (R (%)) and the adsorption capacity (q (mg/g)) are as follows.

The removal efficiency (R (%)) and the adsorption capacity (q (mg/g)) were calculated according to Eqs. (1) and (2) [26–28].

$$R = \frac{C_0 - C_e}{C_0} \times 100\% \quad (1)$$

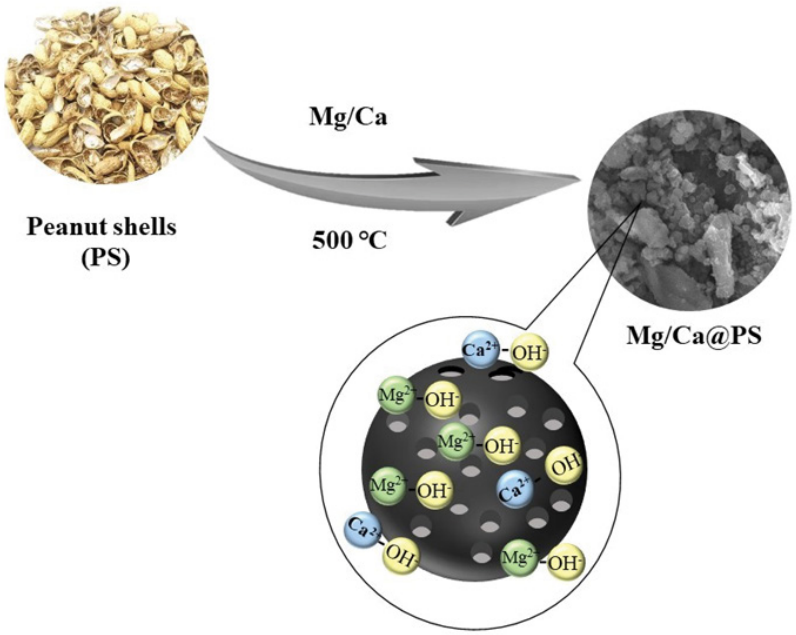

Fig. 1. Synthesis pathway for Mg/Ca@PS.

$$q = \frac{\left(C_0 - C_e\right) \times V}{m} \tag{2}$$

where C_0 (mg/L) and C_e (mg/L) were initial concentration and equilibrium concentration, respectively. V (L) was the solution volume and m (g) was the weight of adsorbent.

3. Results and discussion

3.1. Characteristic of Mg/Ca@PS

SEM images and TEM images of PS and Mg/Ca@PS are shown in Fig. 2.

As shown from Fig. 2, after the peanut shell is pyrolyzed in a muffle furnace under N_2 condition, the surface of the obtained biochar (PS) has a rich irregular structure. The irregular structure will facilitate adsorption. After PS is functionalized with Mg/Ca bimetallic oxide composites, the surface of the obtained composites (Mg/Ca@PS) is rough further. The irregular structure is increased. Some flaky, obvious graininess and flocculent particles appear. It may be the reason that the original pore structure inside the PS is destroyed because of the addition of Mg/Ca bimetallic oxide composites. Additionally, the results indicate that Mg/Ca bimetallic oxide composites appear on the surface of PS. In other words, the PS is successfully modified by Mg/Ca bimetallic oxide composites.

Fig. 3 shows energy-dispersive X-ray analysis (EDS) spectrum and element distribution of PS and Mg/Ca@PS. It can be found that the prepared PS contains the elements of C, O and Si. Their weight percentages are 63.07%, 36.58% and 0.35%, respectively. In additionally, the prepared Mg/Ca@PS contains the elements of C, O, Si, Mg and Ca. Their weight percentages are 55.21%, 39.31%, 0.13%, 2.76% and 2.59%, respectively. As shown from the results of weight percentages, it can be found that the elements of Mg and Ca are appeared on the surface of Mg/Ca@PS. The weight percentage of O is also increased. It indicates that Mg/Ca bimetallic oxide composites are loaded on the surface of PS. This result is consistent with the results of SEM and TEM images.

Fig. 4a shows FT-IR band of PS and Mg/Ca@PS. It can be seen that the trend of the FT-IR band of PS and Mg/Ca@PS is basically the same.

It indicates that PS contains a large of chemical functional groups. It is similar to Mg/Ca@PS. After PS is loaded with Mg/Ca bimetallic oxide composites, its surface chemical functional groups remain unchanged. Seven characteristic adsorption peaks at 3,406; 2,337; 2,002; 1,614; 1,381; 1,100 and 606 cm^{-1} were observed on the surface of Mg/Ca@PS composites. They belong to –OH stretching vibrations, –C≡C– stretching vibrations, –C=C– stretching vibrations, $–CH_2–$ stretching vibrations, –C–O stretching vibrations and –C–H stretching vibrations, respectively [29]. XRD patterns of PS and Mg/Ca@PS are depicted in Fig. 4b. It can be observed that the diffraction peaks are sharp. Additionally, many miscellaneous peaks also can be found on the surface of Mg/Ca@PS. It indicates that the crystallinity of the formed non-unit cell product is higher and the purity of them is lower [30]. The characteristic diffraction peak at 26.26° is observed. It is attributed to the SiO_2 crystal [31]. Four characteristic diffraction peaks at 29.36°, 31.68°, 38.71°, 42.54° and 45.36° appear on the surface of Mg/Ca@PS composites. They are attribute to MgO or $Mg(OH)_2$, and CaO or $Ca(OH)_2$ crystal [32].

According to the results of SEM, TEM, EDS, FT-IR and XRD, it can be concluded that a cost-effective Mg/Ca@PS is obtained. PS is successfully loaded with Mg/Ca bimetallic oxide composites.

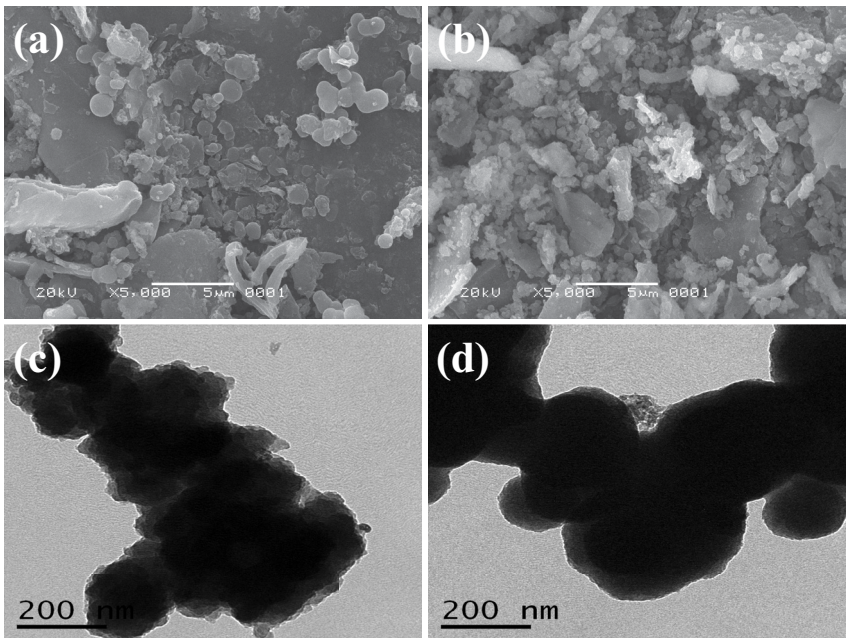

Fig. 2. SEM images of PS (a) and Mg/Ca@PS (b); TEM images of PS (c) and Mg/Ca@PS (d).

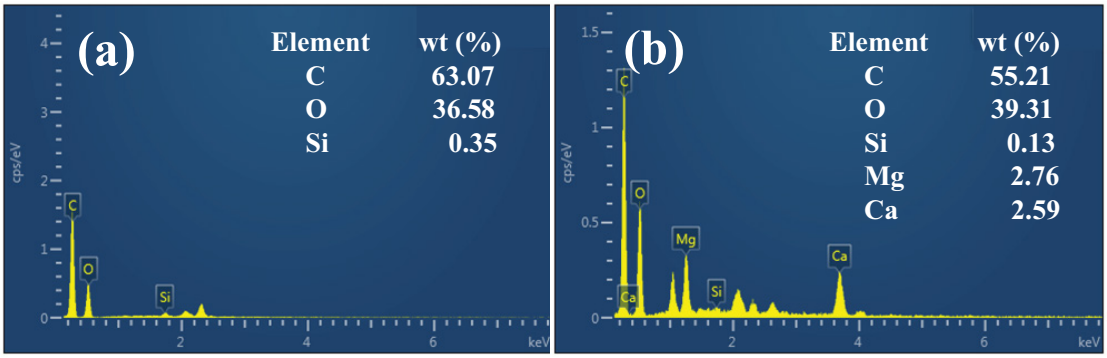

Fig. 3. EDS spectrum and element distribution of PS (a) and Mg/Ca@PS (b).

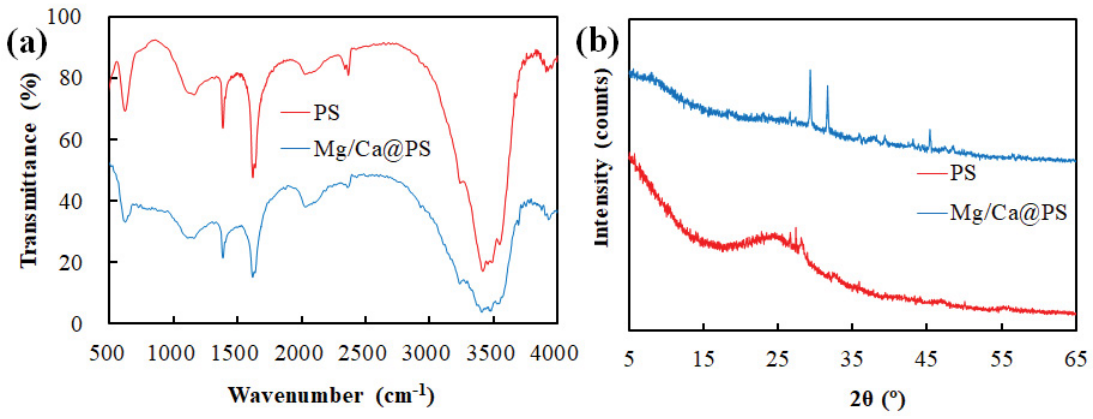

Fig. 4. FT-IR band (a) and XRD patterns (b) of PS and Mg/Ca@PS.

3.2. Effects of operational parameters on NO_3^- and PO_4^{3-} removal in solution

Effects of pH, contact time, concentration of NO_3^- and PO_4^{3-} ions and temperature on NO_3^- and PO_4^{3-} removal in solution by Mg/Ca@PS are shown in Fig. 5. According to the experimental results, it indicates that these operation parameters (pH, contact time, concentration of NO_3^- and PO_4^{3-} ions and temperature) have an important influence on the adsorption capacity of NO_3^- and PO_4^{3-} ions in solution removal by Mg/Ca@PS. From Fig. 5a, it can be seen that pH has an important role during the adsorption process of NO_3^- and PO_4^{3-} ions removal by Mg/Ca@PS. Along with the increase of the initial pH in solution, the adsorption capacity of PO_4^{3-} ions removal by Mg/Ca@PS increases at the first stage. Then, it begins to decrease slowly. When the value of pH is 10, the adsorption capacity of PO_4^{3-} ions removal by Mg/Ca@PS reaches the maximum value. Under a different pH values, there are four main forms of P element in aqueous solutions. They are H_3PO_4, $H_2PO_4^-$, HPO_4^{2-} and PO_4^{3-}, respectively [33].

When pH◎9, Mg/Ca@PS can adsorb $H_2PO_4^-$ and HPO_4^{2-} ions by electrostatic interaction. Furthermore, when the value of initial pH in solution increases, the concentration of OH^- ions in solution also increases. It will lead to the increase of electrostatic repulsion, and compete with phosphorus in solution for adsorption sites. Moreover, it also would react with Ca^{2+} and Mg^{2+} ions to produce precipitation. This would block the pores of Mg/Ca@PS. Therefore, it is not benefit for the adsorption of PO_4^{3-} ions in solution. For NO_3^- ions, as the pH increases, the adsorption capacity NO_3^- ions by Mg/Ca@PS gradually decreases. NO_3^- ions in solution will undergo coordination exchange on the surface of metal oxide hydrates [34]. When the pH of the solution is less than pH_{pzc} value of Mg/Ca@PS, the surface of the Mg/Ca@PS is positively charged. It will facilitate the electrostatic attraction between NO_3^- ions and Mg/Ca@PS. They coordinate exchange with OH^- ions on the surface of Mg/Ca@PS. When the pH of the solution is pH_{pzc} value of Mg/Ca@PS, the surface of Mg/Ca@PS is neutral, and the coordination exchange between NO_3^- ions and OH^- ions occurs directly. When the pH of the solution is more than pH_{pzc} value of Mg/Ca@PS, the surface of Mg/Ca@PS is negatively charged, and it repels electrostatically with NO_3^- ions. Therefore, the probability of coordination exchange between NO_3^- ions and OH^- ions is reduced, resulting in a significant reduction in the removal rate of NO_3^- ions. As shown from Fig. 5a, it depicts that the adsorption capacity of NO_3^- or PO_4^{3-} ions removal by Mg/Ca@PS shows a trend of rapid increase first and then gradually gradual, along with the increase of the concentration of NO_3^- or PO_4^{3-} ions in solution.

It may be the reason that at the initial stage, the number of sites that can be adsorbed and utilized on the surface of Mg/Ca@PS is relatively large [29]. As the contact time increases, the adsorption sites on the surface of Mg/Ca@PS are continuously occupied by NO_3^- or PO_4^{3-} ions in solution. It will lead to a decrease in the driving force of mass transfer, and the rate of adsorption begins to slow down gradually. When the adsorption sites on the surface of the

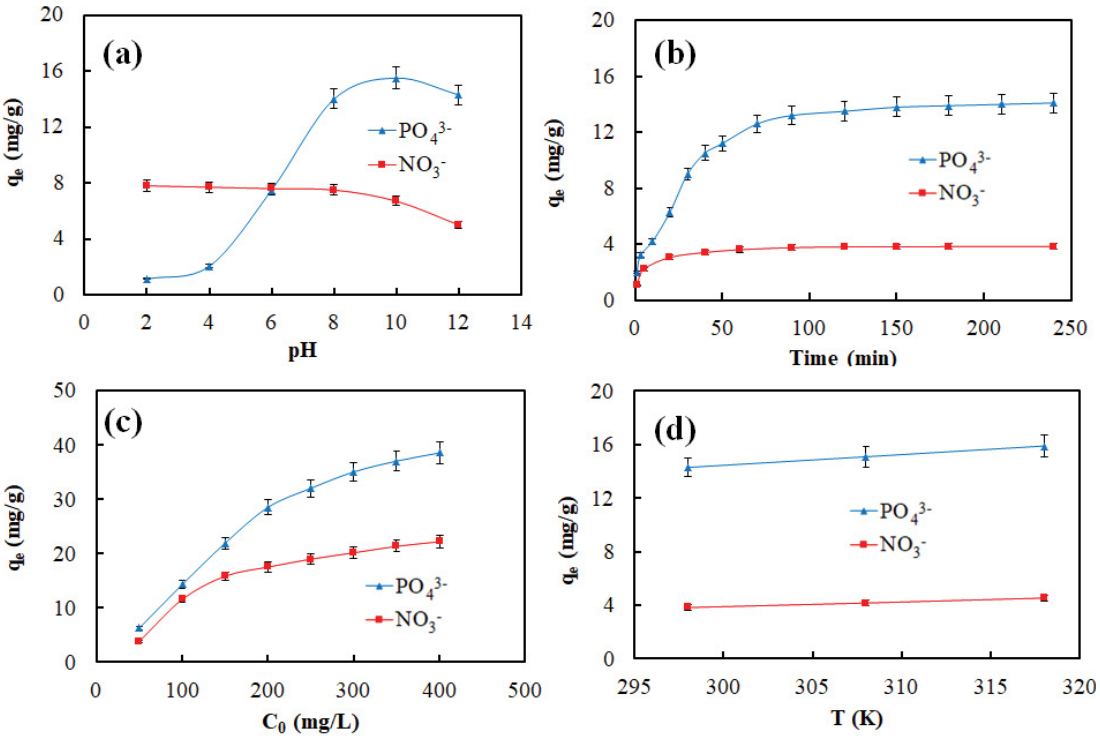

Fig. 5. Effects of operational parameters on NO_3^- and PO_4^{3-} removal in solution (a) pH, (b) contact time, (c) concentration of NO_3^- and PO_4^{3-} and (d) temperature. (Experimental conditions: for PO_4^{3-} ions, 0.1 g Mg/Ca@PS, 20 mL 100 mg/L PO_4^{3-}, contact time of 6 h, pH 8.0, 150 rpm and 25°C; for NO_3^-, 0.2 g adsorbent and 20 mL 50 mg/L NO_3^- ions, contact time of 6 h, pH 2.0, 150 rpm and 25°C).

Mg/Ca@PS tend to be saturated, NO_3^- or PO_4^{3-} ions in solution cannot enter the surface of PS. Then it reaches a state of adsorption equilibrium. The concentration of NO_3^- or PO_4^{3-} ions in solution and temperature are beneficial to the adsorption capacity of NO_3^- or PO_4^{3-} ions in solution removal by Mg/Ca@PS (Fig. 5c and d).

3.3. Kinetic adsorption, the adsorption isotherm and thermodynamic

In order to explore the adsorption mechanism of NO_3^- and PO_4^{3-} ions in solution removal by Mg/Ca@PS, the kinetic adsorption, the adsorption isotherm and thermodynamic are elaborated in details [35,36]. In this work, the kinetic adsorption is depicted by pseudo-first-order kinetic model and pseudo-second-order kinetic model. The adsorption isotherm is depicted by Langmuir isotherm model and Freundlich isotherm model. Thermodynamic parameters are evaluated to determine the spontaneity of the reaction. They are Gibbs free energy ($\Delta G°$ (kJ/mol)), enthalpy ($\Delta H°$ (kJ/mol)) and entropy ($\Delta S°$ (J/mol/K)), respectively.

Eqs. (3) and (4) represent the linear forms of pseudo-first-order and pseudo-second-order kinetic models.

$$q_t = q_e\left(1 - e^{-K_1 t}\right) \tag{3}$$

$$\frac{t}{q_t} = \frac{1}{K_2 q_e^2} + \frac{t}{q_e} \tag{4}$$

where q_e (mg/g) and q_t (mg/g) are adsorption capacity of NO_3^- and PO_4^{3-} ions solution by Mg/Ca@PS at adsorption time t and adsorption equilibrium respectively. K_1 (min^{-1}) and K_2 (min^{-1}) are the adsorption rate constant.

Langmuir isotherm model and Freundlich isotherm model can be expressed in Eqs. (5) and (6). They are as follows:

$$q_e = \frac{q_m C_e K_L}{1 + C_e K_L} \tag{5}$$

where q_e (mg/g) is concentration of adsorbed NO_3^- and PO_4^{3-} ions at equilibrium. q_m (mg/g) is the maximum uptake capacity of N and P. C_e (mg/L) is concentration of TN and TP at equilibrium and K_L (L/mg) is constant.

$$q_e = K_f C_e^{1/n} \tag{6}$$

where q_e (mg/g) is the amount of adsorbed NO_3^- and PO_4^{3-} ions per unit mass of the adsorbent at equilibrium. C_e (mg/L) is concentration of NO_3^- and PO_4^{3-} ions at equilibrium. K_f and $1/n$ are constant.

Thermodynamic parameters can be calculated using Eqs. (7)–(9):

$$\Delta G° = -RT \ln K_a \tag{7}$$

$$\ln K_a = \frac{\Delta S°}{R} - \frac{\Delta H°}{RT} \tag{8}$$

$$K_a = \frac{q_e}{C_e} \tag{9}$$

where T is the solution temperature (K), K_a is the adsorption equilibrium constant, R is the gas constant (8.314 J/mol/K), q_e is the amount of adsorbate adsorbed per unit mass of adsorbate at equilibrium (mg/g) and C_e is the equilibrium concentration of the adsorbate (mg/L). $\Delta S°$ and $\Delta H°$ are calculated from the slope and the intercept respectively.

According the experimental data of Fig. 5b and c and Eqs. (3)–(6), the kinetic adsorption and the adsorption isotherm for NO_3^- and PO_4^{3-} by Mg/Ca@PS are shown in Fig. 6.

Fig. 6a and b show the fitting results of pseudo-first-order kinetic model and pseudo-second-order kinetic model. For adsorption of NO_3^- ions in solution, by comparing the fitting coefficients (R^2), the adsorption process of NO_3^- ions in solution removal by Mg/Ca@PS is better fitted by pseudo-second-order kinetic model (R^2 = 0.9826 < R^2 = 0.9964). Additionally, for adsorption of PO_4^{3-} ions in aqueous solution, the adsorption process also is better fitted by pseudo-second-order kinetic model (R^2 = 0.9735 < R^2 = 0.9953). Therefore, it can be concluded that the adsorption process of NO_3^- or PO_4^{3-} by Mg/Ca@PS is chemical reaction. It is regard as the rate-limiting step. It indicates that the adsorption process contains chemical bonding forces, ion exchange, complexation and precipitation [37]. Additionally, the adsorption capacity of NO_3^- and PO_4^{3-} ions in aqueous solution by Mg/Ca@PS were 18.52 and 47.85 mg/g, respectively. Adsorption capacity comparison of Mg/Ca@PS with the other adsorbents on NO_3^- ions or PO_4^{3-} ions removal is listed in Table 1. The synthesized Mg/Ca@PS possesses an enhanced removal capacity as compared with other materials.

Fig. 6c and d show the fitting results of Langmuir isotherm model and Freundlich isotherm model. It depicts that the adsorption process of NO_3^- ions in solution by Mg/Ca@PS can be described by Langmuir isotherm model (R^2 = 0.9612 > R^2 = 0.8245). It indicates that the adsorption process of NO_3^- ions in solution removal by Mg/Ca@PS is homogeneous monolayers. A lot of uniform adsorption sites appear on the surface of Mg/Ca@PS. For PO_4^{3-} ions in solution, the adsorption process is different. The adsorption process of PO_4^{3-} ions in solution by Mg/Ca@PS can be described by Freundlich isotherm model (R^2 = 0.8733 < R^2 = 0.9059). The adsorption process of PO_4^{3-} ions in solution by Mg/Ca@PS is a multilayer adsorption process.

According to the data from Fig. 5d and Eqs. (7)–(9), the three thermodynamic parameters of $\Delta G°$ (kJ/mol)), enthalpy ($\Delta H°$ (kJ/mol)) and entropy ($\Delta S°$ (J/mol/K) can be calculated. The results are listed in Table S1. Where, $\Delta G° < 0$ shows the adsorption process is a spontaneous nature. The decrease of $\Delta G°$ values with the rising temperature indicates that higher temperature is favorable for the adsorption of NO_3^- and PO_4^{3-} ions in solution by Mg/Ca@PS. Additionally, $\Delta H° > 0$ depicts that the adsorption process is accompanied by endotherm. There may be strong chemical adsorption. Furthermore, $\Delta S° > 0$ indicates that the interface between NO_3^- or PO_4^{3-} ions in solution and Mg/Ca@PS may tend to be disordered [45,46].

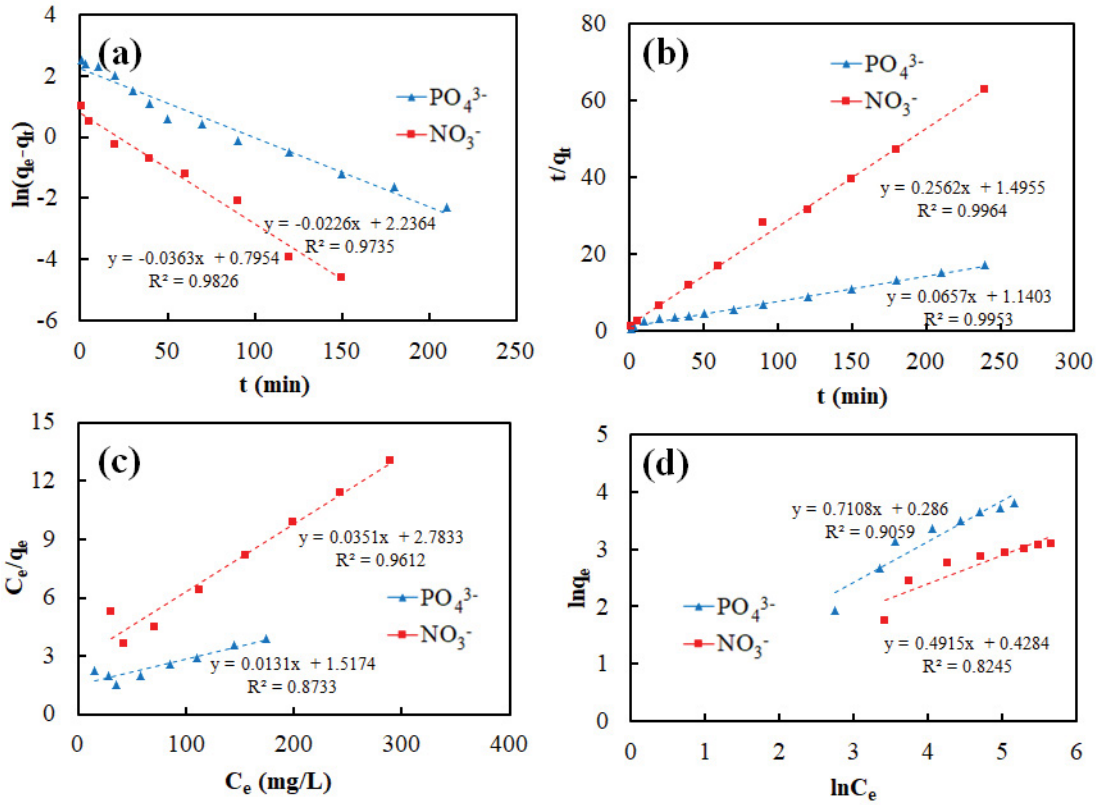

Fig. 6. The adsorption kinetic and the adsorption isotherm for NO_3^- and PO_4^{3-} removal by Mg/Ca@PS (a) pseudo-first-order kinetic model, (b) pseudo-second-order kinetic model, (c) Langmuir isotherm model and (d) Freundlich isotherm model.

Table 1
Adsorption capacity comparison of Mg/Ca@PS with the other adsorbents on NO_3^- ions or PO_4^{3-} ions removal

Adsorbent	Adsorption capacity (mg/g)		Reference
	NO_3^- ions	PO_4^{3-} ions	
LTA MOFs	49.73	62.81	[38]
Al-modified biochar	89.58	57.49	[39]
Modified cellulose from corn stalks	13.60	22.88	[40]
$FeCl_4^-$/Gemini-Mt composite	8.77	28.10	[41]
La_2O_3AM@CS composite beads	27.84	34.91	[42]
Zr@Fu MOF composite	43.97	56.41	[43]
Mg/Al modified biochar	40.63	74.47	[44]
Mg/Ca@PS	18.52	47.85	This work

3.4. Possible reaction mechanism

According to the results of adsorption kinetics, the adsorption isotherm, thermodynamic and the characterization of Mg/Ca@PS, reaction mechanisms of NO_3^- ions or PO_4^{3-} ions removal by Mg/Ca@PS can be depicted as following. For NO_3^- ions, according to the experimental results of the kinetic adsorption, the adsorption isotherm and thermodynamic, the adsorption process of NO_3^- ions in solution by Mg/Ca@PS can be described by pseudo-second-order kinetic model and Langmuir isotherm model, respectively. It indicates that the adsorption process is physic-chemical complex adsorption process dominated by chemisorption. From the characteristics of Mg/Ca@PS, it can be seen that adsorbent of Mg/Ca@PS is high specific surface area, porosity and polarity. It can adsorb the NO_3^- ions in solution by a lot of adsorption sites [47]. The surface adsorption process usually occurs on the surface of Mg/Ca@PS. Additionally, the intraparticle diffusion also can occur on the surface of Mg/Ca@PS, because the prepared material of Mg/Ca@PS is a mesoporous material. The NO_3^- ions are easy to penetrate into the pores of Mg/Ca@PS. The chemical modification of Mg/Ca bimetallic oxide composites functionalized PS makes the surface positively charged [48]. It will cause the electrostatic

attraction to occur. Furthermore, there are a lot of OH^- ions on the surface of Mg/Ca@PS. They can react with NO_3^- ions in solution through ion exchange [49]. In general, the adsorption mechanisms of NO_3^- ions in solution by Mg/Ca@PS mainly contain surface adsorption, intraparticle diffusion, electrostatic attraction and ion exchange.

Additionally, the adsorption mechanisms of PO_4^{3-} ions removal by Mg/Ca@PS are same with the adsorption mechanisms of NO_3^- ions removal. PO_4^{3-} ions can be captured on by various processes [50]. It involves the surface adsorption, intraparticle diffusion, electrostatic attraction and ion exchange. The following reactions are involved in electrostatic attraction between PO_4^{3-} ions and Mg/Ca@PS. They are following as: Mg–O + H_2O^+ → Mg–OH^+ + OH^-, Mg–OH^+ + HPO_4^{2-} → Mg–OH^+ – HPO_4^{2-} and Mg–OH^+ + $H_2PO_4^{2-}$ → Mg–OH^+ – $H_2PO_4^{2-}$. Besides, the adsorption process of PO_4^{3-} ions in solution by Mg/Ca@PS can be described by Freundlich isotherm model. This indicates that it also involves the chemical precipitation of PO_4^{3-} ions with Mg/Ca@PS. On the surface of Mg/Ca@PS, Mg^{2+} ions or MgO nanoparticles will improve PO_4^{3-} ions removal in solution [51]. The main forms of in solution are $H_2PO_4^-$ and HPO_4^{2-}, respectively. Mg^{2+} ions or MgO nanoparticles can react with $H_2PO_4^-$ ions and HPO_4^{2-} ions. The precipitates of $Mg(H_2PO_4)_2$ and $MgHPO_4$ are formed. In other words, the adsorption mechanism of PO_4^{3-} ions removal by Mg/Ca@PS involves chemical precipitation. The reactions are following as [52]: Mg–O + H_2O + $2H_2PO_4^-$ → $Mg(H_2PO_4)_2$ + $2OH^-$, MgO + H_2O → $Mg(OH)_2$(aq), $Mg(OH)_2$(aq) → Mg^{2+} + $2OH^-$, Mg^{2+} + HPO_4^{2-} → $MgHPO_4$ and Mg^{2+} + $2HPO_4^-$ → $Mg(H_2PO_4)_2$. The possible mechanisms of NO_3^- ions or PO_4^{3-} ions removal in solution by Mg/Ca@PS are depicted in Fig. 7.

In summary, Mg/Ca bimetallic oxide composites functionalized peanut shell can effectively remove NO_3^- ions and PO_4^{3-} ions in solution. The adsorption mechanisms of NO_3^- ions and PO_4^{3-} ions in solution by Mg/Ca@PS can be described by surface adsorption, intraparticle diffusion, electrostatic attraction and ion exchange. Moreover, the adsorption mechanism of PO_4^{3-} ions in solution by Mg/Ca@PS also includes chemical precipitation.

3.5. Recycle experiment

In order to investigate the influence of recycle time on removal of NO_3^- or PO_4^{3-} ions in solution by Mg/Ca@PS, a serial of adsorption–desorption experiments are carried out. After Mg/Ca@PS adsorbs the NO_3^- or PO_4^{3-} ions in solution, it is soaked in 250 mL flasks containing of 100 mL 0.1 mol/L HCl for 30 min, and washed for three times by Milli-Q water. Influence of recycle time on the adsorption capacity of NO_3^- and PO_4^{3-} removal in solution by Mg/Ca@PS is displayed in Fig. 8. In the five recycle times, the removal rate of NO_3^- and PO_4^{3-} ions still reaches 55.31% and 48.12%, respectively. It indicates that the chemical stability of Mg/Ca@PS is very well. It is a good reusability environmental friendly material in wastewater treatment of NO_3^- and PO_4^{3-} ions in solution with low-costs.

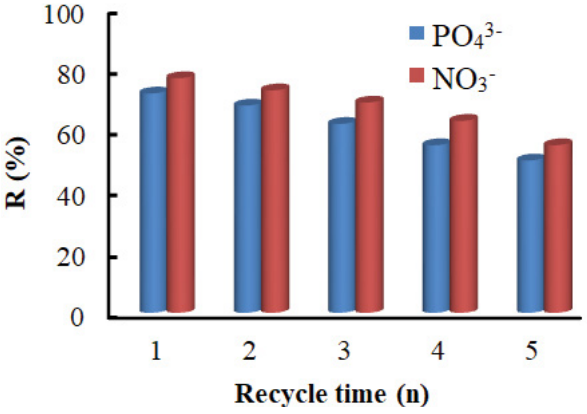

Fig. 8. Influence of recycle time on NO_3^- and PO_4^{3-} removal in solution by Mg/Ca@PS. (Experimental conditions: for PO_4^{3-} ions: 0.1 g Mg/Ca@PS, 20 mL 100 mg/L PO_4^{3-}, contact time of 6 h, pH 8.0, 150 rpm and 25°C; for NO_3^- ions, 0.2 g Mg/Ca@PS, 20 mL 100 mg/L NO_3^- ions, pH 2.0, 150 rpm and 25°C).

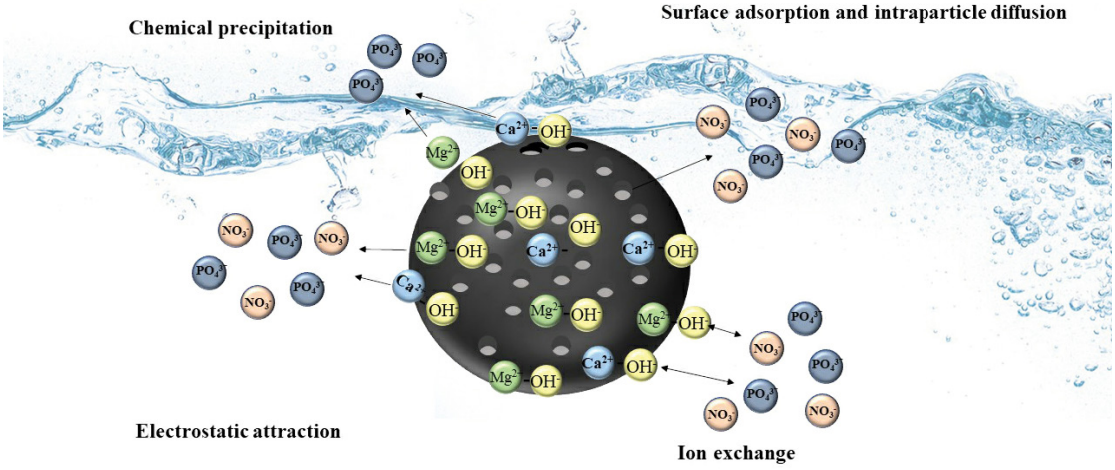

Fig. 7. Possible mechanisms of NO_3^- ions or PO_4^{3-} ions removal in solution by Mg/Ca@PS.

4. Conclusions

In this research, a cost-effective biochar modified by Mg/Ca bimetallic oxide composites (Mg/Ca@PS) is prepared. Biochar of PS from peanut shell is successfully loaded with Mg/Ca bimetallic oxide composites. Mg/Ca bimetallic oxide composites functionalized peanut shell can effectively remove NO_3^- ions and PO_4^{3-} ions in solution. The adsorption process of NO_3^- ions in solution by Mg/Ca@PS is homogeneous monolayers. However, the adsorption process of PO_4^{3-} ions in solution by Mg/Ca@PS is a multilayer adsorption process. Additionally, the adsorption capacity of NO_3^- and PO_4^{3-} ions in aqueous solution by Mg/Ca@PS were 18.52 and 47.85 mg/g, respectively. The adsorption mechanisms of NO_3^- ions and PO_4^{3-} ions in solution by Mg/Ca@PS can be described by surface adsorption, intraparticle diffusion, electrostatic attraction and ion exchange. Moreover, the adsorption mechanism of PO_4^{3-} ions in aqueous solution by Mg/Ca@PS also includes chemical precipitation. The chemical stability of Mg/Ca@PS is very well. It also is a good reusability environmental friendly material in wastewater treatment of NO_3^- and PO_4^{3-} ions in aqueous solution with low-costs.

Acknowledgements

This work is supported by the Natural Science Foundation of Zhejiang Province, China (LGF20C030001) and Guangxi Key Research and Development Program (AB17129002 and AB18050018). Authors are very grateful for their support. We declare that we have no financial and personal relationships with other people or organizations that can inappropriately influence this work.

References

[1] L. Luo, X. Lin, F. Zeng, S. Luo, Z. Chen, G. Tian, Performance of a novel photobioreactor for nutrient removal from piggery biogas slurry: operation parameters, microbial diversity and nutrient recovery potential, Bioresour. Technol., 272 (2019) 421–432.

[2] X. Cui, X. Dai, K.Y. Khan, T. Li, X. Yang, Z. He, Removal of phosphate from aqueous solution using magnesium-alginate/chitosan modified biochar microspheres derived from *Thalia dealbata*, Bioresour. Technol., 218 (2016) 1123–1132.

[3] Q.Q. Yin, B.D. Zhang, R.K. Wang, Z.H. Zhao, Phosphate and ammonium adsorption of sesame straw biochars produced at different pyrolysis temperatures, Environ. Sci. Pollut. Res., 25 (2018) 4320–4329.

[4] M.M.T. Zin, D.-J. Kim, Simultaneous recovery of phosphorus and nitrogen from sewage sludge ash and food wastewater as struvite by Mg-biochar, J. Hazard. Mater., 403 (2021) 123704, doi: 10.1016/j.jhazmat.2020.123704.

[5] L. Luo, G. Wang, G. Shi, M. Zhang, J. Zhang, J. He, Y. Xiao, D. Tian, Y. Zhang, S. Deng, W. Zhou, T. Lan, O. Deng, The characterization of biochars derived from rice straw and swine manure, and their potential and risk in N and P removal from water, J. Environ. Manage., 245 (2019) 1–7.

[6] T. Zhang, X. He, Y. Deng, D.C.W. Tsang, R. Jiang, G.C. Becker, A. Kruse, Phosphorus recovered from digestate by hydrothermal processes with struvite crystallization and its potential as a fertilizer, Sci. Total Environ., 698 (2020) 134240, doi: 10.1016/j.scitotenv.2019.134240.

[7] B. Heibati, S. Rodriguez-Couto, A. Amrane, M. Rafatullah, A. Hawari, M.A. Al-Ghouti, Uptake of Reactive black 5 by pumice and walnut activated carbon: chemistry and adsorption mechanisms, J. Ind. Eng. Chem., 20 (2014) 2939–2947.

[8] E. Rosales, J. Meijide, M. Pazos, M.A. Sanroman, Challenges and recent advances in biochar as low-cost biosorbent: from batch assays to continuous-flow systems, Bioresour. Technol., 246 (2017) 176–192.

[9] K.A. Tan, J. Lalung, N. Morad, N. Ismail, W.M.W. Omar, M.A. Khan, M. Sillanpää, M. Rafatullah, Post-treatment of palm oil mill effluent using immobilised green microalgae *Chlorococcum oleofaciens*, Sustainability, 13 (2021) 11562, doi: 10.3390/su132111562.

[10] P. Hu, Y. Zhang, L. Liu, X. Wang, X. Luan, X. Ma, P.K. Chu, J. Zhou, P. Zhao, Biochar/struvite composite as a novel potential material for slow release of N and P, Environ. Sci. Pollut. Res., 26 (2019) 17152–17162.

[11] K. Premarathna, A.U. Rajapaksha, B. Sarkar, E.E. Kwon, A. Bhatnagar, Y.S. Ok, M. Vithanage, Biochar-based engineered composites for sorptive decontamination of water: a review, Chem. Eng. J., 372 (2019) 536–550.

[12] G. Chen, H. Wang, L. Han, N. Yang, B. Hu, M. Qiu, X. Zhong, Highly efficient removal of U(VI) by a novel biochar supported with FeS nanoparticles and chitosan composites, J. Mol. Liq., 327 (2021) 114807, doi: 10.1016/j.molliq.2020.114807.

[13] M. Hao, M. Qiu, H. Yang, B. Hu, X. Wang, Recent advances on preparation and environmental applications of MOF-derived carbons in catalysis, Sci. Total Environ., 760 (2021) 143333, doi: 10.1016/j.scitotenv.2020.143333.

[14] B. Hu, H. Wang, R. Liu, M. Qiu, Highly efficient U(VI) capture by amidoxime/carbon nitride composites: evidence of EXAFS and modeling, Chemosphere, 274 (2021) 129743, doi: 10.1016/j.chemosphere.2021.129743.

[15] F. Liu, S. Hua, C. Wang, M. Qiu, L. Jin, B. Hu, Adsorption and reduction of Cr(VI) from aqueous solution using cost-effective caffeic acid functionalized corn starch, Chemosphere, 279 (2021) 130539, doi: 10.1016/j.chemosphere.2021.130539.

[16] X. Liu, H. Pang, X. Liu, Q. Li, N. Zhang, L. Mao, M. Qiu, B. Hu, H. Yang, X. Wang, Frameworks-based materials: superior adsorbents for pollutants removal from aqueous solutions, The Innovation, 2 (2021) 100076, doi: 10.1016/j.xinn.2021.100076.

[17] M. Qiu, Z. Liu, S. Wang, B. Hu, The photocatalytic reduction of U(VI) into U(IV) by ZIF-8/g-C_3N_4 composites at visible light, Environ. Res., 196 (2021) 110349, doi: 10.1016/j.envres.2020.110349.

[18] L. Yao, H. Yang, Z. Chen, M. Qiu, B. Hu, X. Wang, Bismuth oxychloride-based materials for the removal of organic pollutants in wastewater, Chemosphere, 273 (2021) 128576, doi: 10.1016/j.chemosphere.2020.128576.

[19] R. Karunanithi, Y.S. Ok, R. Dharmarajan, M. Ahmad, B. Seshadri, N. Bolan, R. Naidu, Sorption, kinetics and thermodynamics of phosphate sorption onto soybean stover derived biochar, Environ. Technol. Innovation, 8 (2017) 113–125.

[20] L. Wu, S. Zhang, J. Wang, X. Ding, Phosphorus retention using iron (II/III) modified biochar in saline-alkaline soils: adsorption, column and field tests, Environ. Pollut., 261 (2020) 114223, doi: 10.1016/j.envpol.2020.114223.

[21] Q. Zheng, L. Yang, D. Song, S. Zhang, H. Wu, S. Li, X. Wang, High adsorption capacity of Mg–Al-modified biochar for phosphate and its potential for phosphate interception in soil, Chemosphere, 259 (2020) 127469, doi: 10.1016/j.chemosphere.2020.127469.

[22] S.V. Novais, M.D.O. Zenero, J. Tronto, R.F. Conz, C.E.P. Cerri, Poultry manure and sugarcane straw biochars modified with $MgCl_2$ for phosphorus adsorption, J. Environ. Manage., 214 (2018) 36–44.

[23] A.A.H. Hakami, S.M. Wabaidu, M.A. Khan, Z.A. Alothman, M. Rafatullah, M.R. Siddiqui, Development of ultra-performance liquid chromatography–mass spectrometry method for simultaneous determination of three cationic dyes in environmental samples, Molecules, 25 (2020) 4564, doi: 10.3390/molecules25194564.

[24] A.A.H. Hakami, M.A. Ahmed, M.A. Khan, Z.A. Alothman, M. Rafatullah, M.A. Islam, M.R. Siddiqui, Quantitative analysis of malachite green in environmental samples using liquid chromatography-mass spectrometry, Water, 13 (2021) 2864, doi: 10.3390/w13202864.

[25] D.A. Munar-Florez, D.A. Varón-Cardenas, N.E. Ramírez-Contreras, J.A. García-Núñez, Adsorption of ammonium and phosphates by biochar produced from oil palm shells: effects of production conditions, Results Chem., 3 (2021) 100119, doi: 10.1016/j.rechem.2021.100119.
[26] H. Shayesteh, A. Rahbar-Kelishami, R. Norouzbeigi, Adsorption of malachite green and crystal violet cationic dyes from aqueous solution using pumice stone as a low-cost adsorbent: kinetic, equilibrium, and thermodynamic studies, Desal. Water Treat., 27 (2016) 12822–12831.
[27] F. Sarbisheh, R. Norouzbeigi, F. Hemmati, H. Shayesteh, Application of response surface methodology for modeling and optimization of malachite green adsorption by modified sphagnum peat moss as a low cost biosorbent, Desal. Water Treat., 59 (2017) 230–242.
[28] P. Koohi, A. Rahbar-Kelishami, H. Shayesteh, Efficient removal of congo red dye using Fe_3O_4/NiO nanocomposite: synthesis and characterization, Environ. Technol. Innovation, 23 (2021) 101559, doi: 10.1016/j.eti.2021.101559.
[29] J. Hou, L. Huang, Z.M. Yang, Y. Zhao, C. Deng, Y. Chen, X. Li, Adsorption of ammonium on biochar prepared from giant reed, Environ. Sci. Pollut. Res., 23 (2016) 19107–19115.
[30] H.G. Zhou, Z.M. Jiang, S.Q. Wei, A novel absorbent of nano-Fe loaded biomass char and its enhanced adsorption capacity for phosphate in water, J. Chem., 21 (2013) 649868, doi: 10.1155/2013/649868.
[31] X.F. Tan, Y.G. Liu, Y.L. Gu, X. Yan, J. Li, Biochar-based nanocomposites for the decontamination of wastewater: a review, Bioresour. Technol., 212 (2016) 318–333.
[32] R. Li, J.J. Wang, B. Zhou, M.K. Awasthi, A. Ali, Z. Zhang, L.A. Gaston, A.H. Lahori, A. Mahar, Enhancing phosphate adsorption by Mg/Al layered double hydroxide functionalized biochar with different Mg/Al ratios, Sci. Total Environ., 559 (2016) 121–129.
[33] K.W. Jung, K.H. Ahn, Fabrication of porosity-enhanced MgO/biochar for removal of phosphate from aqueous solution: application of a novel combined electrochemical modification method, Bioresour. Technol., 200 (2016) 1029–1032.
[34] A. Bhatnagar, E. Kumar, M. Sillanpää, Nitrate removal from water by nano-alumina: characterization and sorption studies, Chem. Eng. J., 163 (2010) 317–323.
[35] H. Shayesteh, A. Rahbar-Kelishami, R. Norouzbeigi, Evaluation of natural and cationic surfactant modified pumice for Congo red removal in batch mode: kinetic, equilibrium, and thermodynamic studies, J. Mol. Liq., 221 (2016) 1–11.
[36] A.H. Alabi, E.O. Oladele, A.J.O. Adeleke, F.C. Oni, C.A. Olanrewaju, Equilibrium, kinetic and thermodynamic studies of biosorption of methylene blue on goethite modified baobab fruit pod (*Adansonia Digitata* L.), J. Appl. Sci. Environ. Manage., 24 (2020) 1229–1243.
[37] W. Yin, D. Dai, J. Hou, S. Wang, X. Wu, X. Wang, Hierarchical porous biocharbased functional materials derived from biowaste for Pb(II) removal, Appl. Surf. Sci., 465 (2019) 297–302.
[38] I.A. Kumar, A. Jeyaseelan, N. Viswanathan, Mu. Naushad, A.J.M. Valente, Fabrication of lanthanum linked trimesic acid as porous metal organic frameworks for effective nitrate and phosphate adsorption, J. Solid State Chem., 302 (2021) 122446, doi: 10.1016/j.jssc.2021.122446.
[39] Q. Yin, H. Ren, R. Wang, Z. Zhao, Evaluation of nitrate and phosphate adsorption on Al-modified biochar: influence of Al content, Sci. Total Environ., 631–632 (2018) 895–903.
[40] C. Fan, Y. Zhang, Adsorption isotherms, kinetics and thermodynamics of nitrate and phosphate in binary systems on a novel adsorbent derived from corn stalks, J. Geochem. Explor., 188 (2018) 95–100.
[41] W. Luo, Q. Huang, P. Zeng, C. Cheng, X. Yuan, T. Xiao, M. Zhang, P. Antwi, J. Xing, S. Ren, Gemini surfactant-modified montmorillonite with tetrachloroferrate ($FeCl_4^-$) as a counter-ion simultaneously sequesters nitrate and phosphate from aqueous solution, J. Hazard. Mater., 409 (2021) 124829, doi: 10.1016/j.jhazmat.2020.124829.
[42] I.A. Kumar, C. Jeyaprabha, S. Meenakshi, N. Viswanathan, Hydrothermal encapsulation of lanthanum oxide derived *Aegle marmelos* admixed chitosan bead system for nitrate and phosphate retention, Int. J. Biol. Macromol., 130 (2019) 527–535.
[43] I.A. Kumar, Mu. Naushad, T. Ahamad, N. Viswanathan, Facile fabrication of tunable porous zirconium fumarate based metal organic frameworks in the retention of nutrients from water, Environ. Sci.: Water Res. Technol., 6 (2020) 2856–2870.
[44] Q. Yin, R. Wang, Z. Zhao, Application of Mg–Al-modified biochar for simultaneous removal of ammonium, nitrate, and phosphate from eutrophic water, J. Cleaner Prod., 176 (2018) 230–240.
[45] P. Wang, L. Tang, X. Wei, G. Zeng, Y. Zhou, Y. Deng, J. Wang, Z. Xie, W. Fang, Synthesis and application of iron and zinc doped biochar for removal of p-nitrophenol in wastewater and assessment of the influence of co-existed Pb(II), Appl. Surf. Sci., 392 (2017) 391–401.
[46] H. Lei, Z. Hao, K. Chen, Y. Chen, J. Zhang, Z. Hu, Y. Song, P. Rao, Q. Huang, Insight into adsorption performance and mechanism on efficient removal of methylene blue by accordion-like V_2CT_x MXene, J. Phys. Chem. Lett., 11 (2020) 4253–4260.
[47] T.T. Wang, D. Zhang, K.K. Fang, W. Zhu, Q. Peng, Z.G. Xie, Enhanced nitrate removal by physical activation and Mg/Al layered double hydroxide modified biochar derived from wood waste: Adsorption characteristics and mechanisms, J. Environ. Chem. Eng., 9 (2021) 105184, doi: 10.1016/j.jece.2021.105184.
[48] S.Y. Lee, J.W. Choi, K.G. Song, K. Choi, Y.J. Lee, K.W. Jung, Adsorption and mechanistic study for phosphate removal by rice husk-derived biochar functionalized with Mg/Al-calcined layered double hydroxides via co-pyrolysis, Composites B, 176 (2019) 107209, doi: 10.1016/j.compositesb.2019.107209.
[49] S.Q. Li, X.L. Ma, Z.C. Ma, X.T. Dong, Z.Y. Wei, X.Y. Liu, L.P. Zhu, Mg/Al-layered double hydroxide modified biochar for simultaneous removal phosphate and nitrate from aqueous solution, Environ. Technol. Innovation, 23 (2021) 101771, doi: 10.1016/j.eti.2021.101771.
[50] J. Zhang, Q. Wang, Sustainable mechanisms of biochar derived from brewers' spent grain and sewage sludge for ammonia–nitrogen capture, J. Cleaner Prod., 112 (2016) 3927–3934.
[51] Y.P. Gong, Z.Y. Ni, Z.Z. Xiong, L.H. Cheng, X.H. Xu, Phosphate and ammonium adsorption of the modified biochar based on *Phragmites australis* after phytoremediation, Environ. Sci. Pollut. Res., 24 (2017) 8326–8335.
[52] Q. Yang, X.L. Wang, W. Luo, J. Sun, Q. Xu, F. Chen, J. Zhao, S. Wang, F. Yao, D. Wang, Effectiveness and mechanisms of phosphate adsorption on iron-modified biochars derived from waste activated sludge, Bioresource Technol., 247(2018)537–544.

Supplementary information

S1. Characterization of sorbents

Scanning electron microscopy (JEOL 6500F, Japan) and transmission electron microscopy (Tecnai G2 20, Netherlands) was used to observe the surface morphology and structure of adsorbents. The surface area and pore size of adsorbents were determined by the NOVA 4200e Surface Area and pore size analyzer (Quantachrome, FL, USA) at a relative pressure of 0.95 following the multipoint N_2-Brunauer–Emmett–Teller adsorption method. The surface functional groups of adsorbents in the wave number range of 500–4,000 cm^{-1} were recorded on a Nexus 670 FT-IR Spectrometer (Thermo Nicolet, Madison). The crystalline structures of the adsorbents were conducted in a D/Max-IIIA Powder X-ray Diffractomer (Rigaku Corp., Japan). XPS (X-ray photoelectron spectrometer, Kratos AXIS Ultra DLD, Japan) and the model Axis-HS (Kratos Analytical) were used to determine the surface of adsorbents.

S2. Adsorption experiments

S2.1. Effect of pH

- 0.1 g adsorbent and 20 mL 100 mg/L PO_4^{3-} ions in solution with different pH (2.0, 4.0, 6.0, 8.0, 10.0 and 12.0) were charged into a series of flasks, respectively. The mixture was shaken at 150 rpm and 25°C for 6 h.
- 0.2 g adsorbent and 20 mL 100 mg/L NO_3^- ions in solution with different pH (2.0, 4.0, 6.0, 8.0, 10.0 and 12.0) were charged into a series of flasks, respectively. The mixture was shaken at 150 rpm and 25°C for 6 h.

S2.2. Effect of initial concentration

- 0.1 g adsorbent and 20 mL initial concentration of PO_4^{3-} ions in solution with a different initial concentration (50, 100, 150, 200, 250, 300, 350 and 400 mg/L) were charged into a series of flasks, respectively. The mixture was shaken at pH 8.0, 150 rpm and 25°C for 6 h.
- 0.2 g adsorbent and 20 mL initial concentration of NO_3^- ions in solution with a different initial concentration (50, 100, 150, 200, 250, 300, 350 and 400 mg/L) were charged into a series of flasks, respectively. The mixture was shaken at pH 2.0, 150 rpm and 25°C for 6 h.

S2.3. Effect of contact time

- 0.1 g adsorbent and 20 mL 100 mg/L PO_4^{3-} ions in solution were charged into a series of flasks, respectively. The mixture was shaken at pH 8.0, 150 rpm and 25°C for different time (1, 3, 10, 20, 30, 40, 50, 70, 90, 120, 150, 180, 210 and 240 min).
- 0.2 g adsorbent and 20 mL 50 mg/L NO_3^- ions in solution were charged into a series of flasks, respectively. The mixture was shaken at pH 2.0, 150 rpm and 25°C for different time (1, 5, 20, 40, 90, 120, 150, 180 and 240 min).

S2.4. Effect of temperature

- 0.1 g adsorbent and 20 mL 100 mg/L PO_4^{3-} ions in aqueous solution were charged into a series of flasks, respectively. The mixture was shaken at pH 8.0 and 150 rpm for 6 h. Temperature is 25°C, 35°C and 45°C, respectively.
- 0.2 g adsorbent and 20 mL 50 mg/L NO_3^- ions in aqueous solution were charged into a series of flasks, respectively. The mixture was shaken at pH 2.0 and 150 rpm for 6 h. Temperature is 25°C, 35°C and 45°C, respectively.

S3. Recycle experiment

- 0.1 g adsorbent and 20 mL 100 mg/L PO_4^{3-} ions in aqueous solution were charged into a series of flasks, respectively. The mixture was shaken at pH 8.0, 150 rpm and 25°C for 6 h.
- 0.2 g adsorbent and 20 mL 100 mg/L NO_3^- ions in aqueous solution were charged into a series of flasks, respectively. The mixture was shaken at pH 2.0, 150 rpm and 25°C for 6 h.

Table S1
Thermodynamic parameters of NO_3^- and PO_4^{3-} ions in solution removal by Mg/Ca@PS

Pollutant	$\Delta G°$ (kJ/mol)			$\Delta H°$ (kJ/mol)	$\Delta S°$ (J/mol/K)
	298 (K)	308 (K)	318 (K)		
NO_3^-	–2.79	–1.76	–0.097	42.86	134.08
PO_4^{3-}	–1.71	–1.24	–0.67	17.14	51.74